Combining magnetic nanoparticles and icosahedral boron clusters in biocompatible inorganic nanohybrids for cancer therapy

Combining Magnetic Nanoparticles and Icosahedral Boron Clusters in Biocompatible Inorganic Nanohybrids for Cancer Therapy.

Elena Oleshkevich[a], Anna Morancho[b], Arpita Saha[a], Koen M. O. Galenkamp[c,d,e], Alba Grayston[b], Simonetta Geninatti Crich[f], Diego Alberti[f], Nicoletta Protti[g], Joan X. Comella[c,d,e], Francesc Teixidor[a], Anna Rosell[b,*], Clara Viñas[a,*].

[a] Institut de Ciència de Materials de Barcelona (ICMAB-CSIC), Bellaterra, Spain. [b] Neurovascular Research Laboratory, Vall d'Hebron Research Institute, Universitat Autònoma de Barcelona. Barcelona. [c] Cell Signaling and Apoptosis Group, Vall d'Hebron Research Institute, Barcelona, Spain. [d] Institut de Neurociències, Departament de Bioquímica i Biologia Molecular, Facultat de Medicina, Universitat Autònoma de Barcelona, Bellaterra, Spain. [e] Centro de Investigación Biomédica en Red sobre Enfermedades Neurodegenerativas (CIBERNED), Madrid, Spain. [f] Department of Molecular Biotechnology and Health Sciences, University of Torino. Torino, Italy. [g] Department of Physics, University of Pavia. Pavia, Italy.

Corresponding Authors: Dr. Clara Viñas, clara@icmab.es, Institut de Ciència de Materials de Barcelona (ICMAB-CSIC), Campus U.A.B. 08193 Bellaterra, Spain. +34 935801853. and Dr. Anna Rosell, anna.rosell@vhir.org, Vall d'Hebron Research institute, Passeig Vall d'Hebron 119-129, 08035, Barcelona, Spain. +34 934894029.

Conflicts of interest: the authors declare no conflicts of interest.

Financial support: This work has been supported by the Spanish Ministerio de Economía y Competitividad (CTQ2016-75150-R, SAF2016-80236-R, CIBERNED CB06/05/1104), Generalitat de Catalunya (2017 SGR 1720, SGR 1427); Miguel Servet program (CPII15/00003), PFIS grant (FI17/00073), from Fondo de Investigaciones Sanitarias-Instituto de Salud Carlos III and ERDF. E. O. thanks FPU predoctoral grant.

Word count for abstract: 150

Word count for manuscript: 3,688

Number of References: 60

Number of Figures: 8

Number of Tables: 1

Number of Supplementary online-only files: 1

ABSTRACT

The potential biomedical applications of the MNPs nanohybrids coated with *m*-carboranylphosphinate (**1**-MNPs) as a theranostic biomaterial for cancer therapy were tested. The cellular uptake and toxicity profile of **1**-MNPs from culture media by human brain endothelial cells (hCMEC/D3) and glioblastoma multiform A172 cell line was demonstrated. Prior to testing **1**-MNPs' *in vitro* toxicity, studies of colloidal stability of the **1**-MNPs' suspension in different culture media and temperatures were carried out. TEM images and chemical titration confirmed that **1**-MNPs penetrate into cells. Additionally, to explore **1**-MNPs' potential use in Boron Neutron Capture Therapy (BNCT) for treating cancer locally, the presence of the *m*-carboranyl coordinated with the MNPs core after uptake was proven by XPS and EELS. Importantly, thermal neutrons irradiation in BNCT reduced by 2.5 the number of cultured glioblastoma cells after **1**-MNP treatment, and the systemic administration of **1**-MNPs in mice was well tolerated with no major signs of toxicity.

Keywords. *m*-carboranyl, phosphinate, iron oxide nanoparticles, Boron Neutron Capture Therapy, nanomedicine.

BACKGROUND

The synthesis of magnetic nanoparticles (MNPs) has been intensively developed for many technological[1] and medical applications.[2,3] Typical MNPs obtained by bottom up synthesis consist of a magnetic core and an organic or inorganic shell that provides a barrier between the core and its environment dispersing them in water at a range of different pH, among other tasks. While MNPs' physical properties are determined by their inorganic magnetic core, their surface properties also play an important role, especially in effective interfacing (e.g., ensuring biocompatibility and specific site) with biological systems. Superparamagnetic iron oxide nanoparticles (SPIONs or MNPs) have been extensively investigated for numerous *in vivo* and *in vitro* applications, such as magnetic resonance imaging (MRI) contrast enhancement,[4] tissue repair, detoxification of biological fluids, hyperthermia, drug delivery, immunoassays and cell separation techniques.[2]

All these biomedical applications require that MNPs have high magnetization values, a size smaller than 100 nm, and a narrow particle size distribution. These applications also require a demanding surface coating of the MNPs, which has to be nontoxic and biocompatible.[5] Such MNPs have been bound to drugs, proteins, enzymes, antibodies, or nucleotides and can be directed to an organ, tissue, or tumour using an external magnetic field.[6,7] However, only one example of *o*-carborane cages attached to MNPs through a long linker for cancer treatment can be found in the literature.[8] Among different surface coating *o*-carborane cages, carboranylphosphinates,[9] have many advantages due to their good affinity towards MNPs, their highly

biocompatible tridimensional structure and their high boron content, that can be exploited for Boron Neutron Capture Therapy(BNCT) which is based on the nuclear capture and fission reactions that occur when the stable isotope ^{10}B is irradiated with epithermal neutron beam radiation in clinical use, which become thermalized as they penetrate tissue.[10]

The most studied carborane is 1,2-dicarba-*closo*-dodecaborane, 1,2-*closo*-$C_2B_{10}H_{12}$, and its isomers (1,7 and 1,12-) that can be viewed as 3D aromatic systems[11] whose volume approximates to that of one displayed by a benzene molecule rotating on one of its twofold axes.[12] These carboranes exhibit an unusual combination of properties such as low nucleophilicity, chemical inertness, thermal stability,[13,14] as well as stability and low toxicity in biological systems.[15-21] The rigid geometry and the relative easy functionalization at the carbon vertexes of the carborane cluster[13,22,23] allow the preparation of a wide number of compounds potentially useful as precursors of more complex materials.[24-29] Furthermore, the use of carboranes in supramolecular chemistry is a topic, which raises great interest for their particular properties [12,30-34] that may induce an unexpected behaviour in the supramolecular structures in which they are inserted. Our vision of the carboranyl substituent, however, is that it is unique as a ligand because it is a hollow rigid sphere appended to a metal coordinating site. This, along with its hydrophobicity and electron withdrawing properties through the carbon cluster, C_c,[35-37] suggests the possibility of inducing distinct geometrical behaviour in boron rich macromolecules or particles of significance for Boron Neutron Capture Therapy (BNCT),[38-44] an alternative

radiotherapy used for aggressive and infiltrating types of cancer that can not be treated with surgery or standard radio or chemotherapy, and by drug delivery.[45,46]

The theoretical advantage of BNCT is that it can selectively destroy tumour cells infiltrating normal tissue with the requirement that sufficient amounts of ^{10}B and thermal neutrons are properly delivered to the site of the tumour.[38-46] Clinical interest in BNCT has focused primarily on high grade gliomas and on recurrent tumours of the head and neck region who have failed conventional therapy. BNCT integrates the focusing approach of chemotherapy and the gross anatomical localization advantage of traditional radiotherapy, offering the ability to deposit an immense dose-gradient between the tumour cells and normal cells.[47] For this, new and better boron delivery agents targeting cancer cells are needed for the clinical use.

Particularly in this work, the carborane derivative utilized, is *m*-carboranylphosphinate and its acid form that is *m*-carboranylphosphinic acid (Figure1), which was recently reported.[9] The ligand is subjected to the properties bestowed by the *m*-carborane, though the most notable properties in reference to the results obtained in this work are the reduced tendency of the phosphinate coordinated group to be oxidized (a property which is uncommon among organic phosphinates), the spherical nature of the carborane (driving to space-filling efficiency) and the hydrophobicity of the carboranyl unit.

In this paper, we have assessed the *in vitro* and *in vivo* properties of the boron cluster-MNPs nanohybrids coated with *m*-carboranylphosphinate ([**1**]$^-$), which were prepared (**1**-MNPs)[48] by the classic co-precipitation synthesis**.**

To illustrate their potential biomedical applications, we have demonstrated the cellular uptake of these **1**-MNPs from culture media by a tumour glioblastoma cell line (A172) and in a human cell line of capillary-derived human brain endothelial cells (hCMEC/D3) as normal tissue cells. We show by TEM images that the **1**-MNPs penetrate into these cells in membrane vesicles and remain within the cell cytoplasm. Additionally, their potential ability to penetrate into malignant glioblastoma cells as boron carriers for selective cancer treatment with BNCT is explored together with the in vivo tolerance after intravenous administration. Based on the presented results, the bifunctional MNPs nanohybrids coated with *m*-carboranylphosphinate are new nanomaterials that could act in dual therapies (BNCT and thermotherapy) with the aim to obtain the best therapeutic effects using the lowest doses and therefore avoiding unwanted organism toxicity and side effects in healthy tissues.

METHODS

The conducted study overlaps nanoscience experiments (stability studies of coated MNPs with Boron clusters) with functional *in vitro* and *in vivo* experiments (cellular uptake and imaging, BNCT irradiation in glioblastoma cells, and nanohybrid biocompatibility in mice) including: Dynamic Light Scattering (DLS) and Zeta Potential; Superconductive Quantum Interference Device (SQUID) magnetometer (Quantum Design MPMS5XL); TEM of cells; preparation of **1**-MNPs aqueous suspension at the physiological pH; cellular uptake of **1**-MNPs; cell viability assays;

cell count; dried cells preparation for magnetization measurements, XPS, HRSTEM, EELS and EFTEM studies; cytoplasmic **1**-MNPs detection by Prussian blue and **1**-MNPs visualization by Transmission Electron Microscopy (TEM); Magnetic Resonance Imaging (MRI); Boron and Iron determination by Inductively Coupled Plasma Mass Spectrometry (ICP-MS) analysis; Cell irradiation and proliferation assays and "*in vivo*" **1**-MNPs administration in mice. Detailed descriptions can be found in the S.I. Animal procedures for the MNPs administration were approved by the Ethics Committee of Animal Experimentation of the Vall d'Hebron Research Institute and were conducted in compliance with Spanish legislation and in accordance with the Directives of the European Union. A detailed description of the techniques and conducted experiments can be found in the supplementary information (S.I).

The uptake of **1**-MNPs was measured through the MNPs core and calculated as follows: first, dividing the MR value of the treated cells by the total number of cells at 5K, which provides the magnetization per cell (emu/cell), then further dividing this value by the remanent magnetization of the **1**-MNPs (emu/g $_{\mathbf{1}\text{-MNPs}}$) at 5K to obtain the amount of iron per cell.

RESULTS

Colloidal stability of the 1-MNPs suspension.

The stability of the colloidal dispersions of **1**-MNPs (50 μg **1**-MNPs/mL) was studied by DLS in different culture media (DMEM-F12-1% FBS, DMEM-1% FBS, EGM2-

2%FBS and RPMI) and as well as in phosphate-buffered saline (PBS) solution that contains inorganic salts (NaCl, Na_2HPO_4, KH_2PO_4, KCl) at different time intervals (10 min. and 24 h.) and temperatures (r.t. and 37°C). The results are on display in Table 1.

In all tested culture media no precipitation was observed neither after 10 min nor after incubating 24 h at r.t. or at 37ºC, while in PBS **1**-MNPs sediment within 24 h at r.t. In the case of DMEM F12-1% FBS, 1% non-essential amino acids and 1% antibiotics, and in RPMI the size of detected particles was close to the mean particle diameters determined by TEM, $Ø_{TEM}$ = 7.6±0.6 nm. In EGM-2 medium with 2%FBS and in DMEM-1%FBS **1**-MNPs rapidly formed aggregates with hydrodynamic diameters in the range of 50-140 nm and 60-170 nm, respectively, maintaining an invariable size for 24 h. Comparing results at r.t. and 37ºC, a slight increase in hydrodynamic diameters was observed in all culture media (Table 1). To know more about the stability of **1**-MNPs in PBS, DLS measurements at 10 and 30 minutes as well as at 2, 4 and 8 hours were conducted (see S. I.).

Determination of 1-MNPs uptake by endothelial and glioblastoma cells.

The first step of the biological studies was to confirm the uptake of the sterilized **1**-MNPs by the cultured cells (hCMEC/D3 and A172). As shown in the right panels of Figure 2, the Prussian blue stain enables us to identify the presence of intracellular iron after 24 h treatment with **1**-MNPs. Cell viability assay also shows that brain endothelial (hCMEC/D3) cells were more sensitive to **1**-MNP toxicity than glioblastoma A172 cells (Figure 2A and 2B) since doses of 25 μg $Fe^{2+/3+}$/mL

significantly reduced endothelial cell viability. The reduction in hCMEC/D3 viability could be only partially explained by the vehicle solution consisting in equal content of *m*-carboranylphosphinic acid (H[**1**]) and [NMe_4]OH as in a **1**-MNPs colloidal suspension, but certainly the **1**-MNPs nanohybrid induced cell toxicity starting at 25 μg/mL. Under the same administered doses of **1**-MNPs, glioblastoma A172 cells presented full viability as observed in Figure 2B. However, higher doses induced cell toxicity to the cancer cells, maybe due to the acidity of *m*-carboranylphosphinic acid present in the vehicle solution**.** These results provide a prove of dose-dependent effects of the **1**-MNPs compound in normal tissue (endothelial) and tumour cells (glioblastoma) which are considered for further **1**-MNPs loading experiments.

Quantification of the cellular 1-MNPs uptake.

To confirm the uptake of MNPs core by the A172 and hCMEC/D3 cells after 6 or 24 h of incubation in the presence of **1**-MNPs, the cells were dried, as described in the experimental section and the magnetism measurements were run (see the S. I.). The results determine the amount of iron per cell and show a clear time and dose-dependent relationship with both endothelial and glioblastoma cell lines as shown in Figure 3A. Moreover, with the same dose of **1**-MNPs (25 ug/ml) A172 cells presented larger cellular iron content than endothelial cells (6-fold and 4-fold increase after 6 and 24 hours, respectively) as shown in Figure 3B, indicating a higher capacity of cellular load with iron oxides without toxic effects (Figure 3). These are interesting results suggesting that by using low doses of **1**-MNPs, glioblastoma

cancer cells may be largely loaded with the **1**-MNPs compound compared to other healthy neighbouring cells in the tissue such as endothelial cells.

Cell Visualization of 1-MNPs uptake.

The presence of cytoplasmic **1**-MNPs core and its intracellular localization into hCMEC/D3 and A172 cells was visualized by TEM analysis in membrane-bound compartments matching with endosomal or lysosomal organelles (Figure 4) at least 24 hours after labelling, as described for other iron oxide compounds.[49-51] This result confirms the cellular load with the **1**-MNP compound and confirms the cell-dependant **1**-MNP load, being higher in A172 glioblastoma cells.

Additionally, to assess whether the amount of Fe internalized in A172 cells was enough to allow MRI visualization on a T_2-weighted image, cells were incubated in the presence of **1**-MNPs (25 and 50 µg/mL Fe) for 6 or 24h and prepared for MRI as described in the S.I. As shown in Figure 4 the acquired signal intensity is dramatically lower (hypointense) in all the treated samples with respect to non-treated control cells. This opens the opportunity to use MRI to carry out a non-invasive quantification of Fe and consequently Boron taken up by target cells, respectively.

However, the presence of the *m*-carboranyl cluster surrounding the observed MNPs core present in the glioblastoma A172 cytoplasm could not be confirmed by EELS and EFTEM elemental maps, probably because of the low levels of boron, thus only Fe was clearly detected (see S. I.). To overcome this drawback and to unambiguously prove the presence of the *m*-carboranyl cluster coordinated at the MNPs core, high resolution XPS and EELS spectra on the A172 dried-cells sample were done. Peaks

at 189 and 133 eV in the XPS analysis, which are characteristic of B-B[52] and P-O bonding, were observed and that clearly confirmed the presence of *m*-carboranyl phosphinate coordinated to the MNP core (Figure 5). EELS analysis on the A172 dried-cells sample also shows the B-K and PL2,3 edges present in the sample proving that the carboranylphosphinate coordinates to MNPs surface**.**

Cell toxicity to the ligand shell coating of 1-MNPs.

Finally, the toxicity of the ligand shell coating the MNPs core (Na[**1**] salt) was determined in both A172 and hCMEC/D3 cells in a dose-response cell viability assay. As observed for the whole **1**-MNPs compound, endothelial cells were more sensitive to the Na[**1**] salt than the glioblastoma cells since Lethal Dose 50 was around 1 mM compared to the 7.5 mM observed in A172 cells; see Figure 6A and 6B. Those doses correspond to 230 $\mu g_{Na[1]}$/mL and 1725 $\mu g_{Na[1]}$/mL of Na[**1**], respectively**.**

Cell neutron irradiation.

BNCT studies were carried out incubating A172 cells for 24h with **1**-MNPs (20 μg/mL Boron). The amount of internalized Boron measured by ICP-MS was of 133±25 μg/g corresponding to a ^{10}B concentration of 26±5 μg/g. Using the above mentioned condition, two groups of A172 cells were irradiated for 15 min in the thermal column of the TRIGA Mark II reactor at the University of Pavia (Reactor Power 30 kW): untreated control cells and **1**-MNPs-treated cells. These were further compared with the respective non-irradiated controls. The proliferation rate (Figure 7) of irradiated and **1**-MNPs treated cells re-plated the day after BNCT is

considerably lower than both control cells, thus demonstrating the efficacy of **1**-MNPs as boron carriers for this cancer therapy. On day 6, BNCT irradiation reduced by 2.5 the number of cancer cells treated with **1**-MNP when compared to non-treated cells**.**

Evaluation of in vivo toxicity of the 1-MNP compound in mice.

We aimed at proving for the first time that the **1**-MNPs were well-tolerated and did not induce major acute toxicity signs such as death, seizures or convulsions but also acute pain, distress, decreased/increased motor activity or dehydratation by monitoring body weight before and after treatment. Briefly, mice received 80 μL of **1**-MNPs intravenously that corresponds to 0.58±0.03 mg/kg of body weight, very close to the approved dose for Feridex® in humans (0.56 mg/Kg of body weight) and previously tested in other "*in vivo"* studies.[53] Importantly, all mice survived the study period (10 days) with no major signs of toxicity. In particular, we found that the individual body weight of the 2 treated groups were comparable with the control group (naïve mice) with day to day fluctuations but without showing significant differences between groups in the body weight ($p = 0.9$; Figure 8A)**.**

DISCUSSION

The development of multifunctional hybrid nanomaterials which could be applied in multi-modal treatments to obtain more efficient drugs with diminishing secondary effects is of great interest nowadays. Thus, based on the biofunctional properties of the multifunctional hybrid nanomaterials, our aim in the present study was to prepare

MNPs coated with *m*-carboranylphosphinate ([**1**]$^-$)) to be applied as a theranostic biomaterial for cancer therapy: biocompatible agents for cell labelling used for both tracking purposes and BNCT treatments

The present study shows that the newly synthesized nanohybrid **1**-MNPs could be used to target cancer cells for tumour imaging and treatment with BNCT therapy. This technique is a highly selective type of radiation therapy that can target tumour cells without causing radiation damage to the adjacent normal cells. Specifically, the **1**-MNPs compound is taken up from culture media by glioblastoma multiform cell line A172 in a higher amount than in the endothelial cells with cell-tracking properties due to the magnetic core of **1**-MNPs by showing a reduced signal on T_2 weighted Magnetic Resonance Imaging (MRI). This characteristic could allow the indirect quantitative determination of boron at the target site before and during neutron irradiation becoming an advantage during cancer treatment since it allows the determination of the optimal neutron irradiation time and a precise calculation of the delivered dose.[54,55] Moreover, BNCT was performed on A172 cells treated with **1**-MNPs, demonstrating the eligibility of **1**-MNPs as boron vectors for an efficient BNCT. Finally, it was assessed that the systemic administration of these **1**-MNPs in adult mice is well tolerated at mid-term with no major signs of toxicity.

It has been recently reported that pH produces an effect on the hydrodynamic radius of aqueous **1**-MNPs suspensions and many studies have revealed that MNPs behave differently in biological media than in water at physiological pH (7.45)[56] because of

the presence of inorganic salts, proteins, amino acids or polysaccharides in biological media.[57] Our newly synthesized boron nanohybrids **1**-MNPs showed colloidal stability in different culture media and at temperatures (room temperature and 37°C) and a nanometric size, supporting their use in biological studies**.**

The hybrid nature of MNPs is conceptually divided into the inorganic core, the engineered surface coating comprising the ligand shell and the corona of adsorbed biological molecules. Empirical evidence shows that all three components may degrade individually *in vivo* and can drastically modify the life cycle and biodistribution of the whole heterostructure.[5,6,7] Thus, MNPs may be decomposed into different parts, whose biodistribution and fate would need to be analysed individually. In this regard, functional studies confirmed the uptake of **1**-MNPs by the cultured cells by Prussian blue staining identifying the presence of intracellular iron after 24 h treatment with **1**-MNPs. These experiments suggest that there has been cytoplasmic endocytosis of the iron core of the **1**-MNPs, as previously described for other iron oxide nanoparticles by other authors.[58,59] These findings were further confirmed by electron microscopy on both endothelial and glioblastoma cells treated with **1**-MNPs showing internalized iron particles in membrane vesicles (endosomes/lysosomes).

On the other hand, high resolution XPS and EELS spectra on the A172 dried-cells sample unambiguously proved the presence of the *m*-carboranylphosphinate;peaks at 189 and 133 eV, which are characteristic of B-B[52] and P-O bonding, thus, confirming the presence of boron cluster ligands in the treated cells. Quantification

of **1**-MNPs uptake by cells displayed that glioblastoma A172 cells presented larger cellular iron contents than brain endothelial (hCMEC/D3) cells when treated at similar conditions of the **1**-MNPs compound, suggesting that by using low doses of MNPs, glioblastoma cancer cells might be largely labelled with the **1**-MNPs compound compared to other neighbouring cells more sensitive to the compound such as endothelial cells. These newly synthesized boron nanohybrids have significant biocompatible properties at certain administered doses allowing cell labelling with potential applications to penetrate into malignant tumour cells as drug carriers or for Boron Neutron Capture Therapy. The amount of both Fe and Boron internalized by A172 tumour cells in our study are sufficient to allow a successful MRI guided BNCT since it exceeds the minimum amount of ^{10}B necessary to perform BNCT[60]. Moreover, nanoparticles could also be prepared using ^{10}B enriched carboranes to improve the toxic effect of neutrons.

Importantly, in terms of drug safety we have shown that the systemic administration of the **1**-MNPs nanohybrids does not show major signs of toxicity in mice, supporting its potential translation into the biomedical setting. This is a preliminary but relevant result before moving to the efficacy studies in the pre-clinical setting using tumour models in rodents.

In conclusion, we believe that these new boron cluster-MNPs nanohybrids, **1**-MNPs, might offer a broad scope for exciting research and future biomedical applications, including cancer therapy**.**

Electronic Supplementary Information (S.I) is available.

REFERENCES

1. Faivre D, Bennet M. Magnetic nanoparticles line up. *Nature* 2016;**535**:235-36.
2. Pankhurst QA, Thanh NTK, Jones SK, Dobson J. Progress in applications of magnetic nanoparticles in biomedicine. *J Phys D: Appl Phys* 2009;**42**(22):224001-16.
3. Lee N, Yoo D, Ling D, Cho MH, Hyeon T., Cheon J. Iron Oxide Based Nanoparticles for Multimodal Imaging and Magnetoresponsive Therapy. *Chem Rev* 2015;**115**:10637-89.
4. Casula MF, Floris P, Innocenti C, Lascialfari A, Marinone M, Corti M, et al.. Magnetic Resonance Imaging Contrast Agents Based on Iron Oxide Superparamagnetic Ferrofluids.. *Chem Mater* 2010;**22**:1739-48.
5. Feliu N, Docter D, Heine M, del Pino P, Ashraf S, Kolosnjaj-Tabi J, et al.. In vivo degeneration and the fate of inorganic nanoparticles. *Chem Soc Rev* 2016;**45**(9):2440-57.
6. Berry CC. Progress in functionalization of magnetic nanoparticles for applications in biomedicine. *J Phys D: Appl Phys* 2009;**42**:224003-(9pp).
7. Majewski P, Thierry B. Functionalized Magnetite Nanoparticles-Synthesis, Properties, and Bio-Applications. *Crit Rev Solid State Mater Sci* 2007;**32**:203-15.
8. Zhu Y, Lin Y, Zhu YZ, Lu J, Maguire JA, Hosmane NS. Boron Drug Delivery via Encapsulated Magnetic Nanocomposites: A New Approach for BNCT in Cancer Treatment. *J Nanomater* 2010;409320-27.

9. Oleshkevich E, Teixidor F, Choquesillo-Lazarte D, Sillanpää R, Viñas C. Carboranylphosphinic Acids: A New Class of Purely Inorganic Ligands. *Chem Eur J* 2016;**11**:3665-70.
10. Barth RF, Mi P, Yang W. Boron delivery agents for neutron capture therapy of cancer. *Cancer Commun.* 2018;**38**:35(15 pages).
11. Poater J, Solà M, Viñas C, Teixidor F. π aromaticity and three-dimensional aromaticity: two sides of the same coin? *Angew. Chem Int Ed*, 2014;**53**(45):12191-5.
12. Scholz M, Hey-Hawkins E. Carbaboranes as Pharmacophores: Properties, Synthesis, and Application Strategies. *Chem Rev* 2011;**111**:7035-62.
13. Grimes RN. Carboranes 3rd Ed.: Elsevier Inc., New York/Oxford, 2016. Plesek J. Potential applications of the boron cluster compounds. *Chem Rev* 1992;**92**:269-78.
14. Plesek J. Potential applications of the boron cluster compounds. *Chem. Rev.* 1992;**92**:269-78.
15. Lesnikowski ZJ. Challenges and Opportunities for the Application of Boron Clusters in Drug Design. *J Med Chem* 2016;**59**:7738-58.
16. Samman S, Foster M, Hunter D. in Boron Science: New Technologies and Applications, (Ed: N. S. Hosmane), CRC Press Ed., Boca Raton, 2012, 73-84.
17. Soloway AH, Tjarks W, Barnum BA, Rong F-G, Barth RF, Codogni IM, et al. The Chemistry of Neutron Capture Therapy. *Chem Rev* 1998;**98**:1515-62.

18. Valliant JF, Guenther KJ, King AS, Morel P, Schaffer P, Sogbein OO, et al. The medicinal chemistry of carboranes. Coord. *Chem Rev* 2002;**232**:173-230.
19. Julius R, Farha O, Chiang J, Perry L, Hawthorne MF. Synthesis and evaluation of transthyretin amyloidosis inhibitors containing carborane pharmacophores. *Proc Natl Acad Sci U.S.A.* 2007;**104**:4808-13.
20. Boron-Based Compounds: Potential and Emerging Applications in Medicine (Eds. C. Viñas and E. Hey-Hawkins), John Wiley & Sons Ltd, Chichester, U.K., 2018.
21. Fuentes I, Garcia-Mendiola T, Sato S, Pita M, Nakamura H, Lorenzo E, Teixidor F, Marques F, Viñas C. Metallacarboranes on the Road to Anticancer Therapies: Cellular Uptake, DNA Interaction, and Biological Evaluation of Cobaltabisdicarbollide [COSAN]$^{-}$. *Chem Eur J* 2018;**24**:17239-54.
22. Bregadze VI. Dicarba-closo-dodecaboranes C2B10H12 and their derivatives. *Chem Rev* 1992;**92**:209-23.
23. Olid D, Núñez R, Viñas C, Teixidor F. Methods to produce B-C, B-P, B-N and B-S bonds in boron clusters. *Chem Soc Rev* 2013;**42**:3318-36.
24. Peterson JJ, Werre M, Simon YC, Coughlin EB, Carter KR. Carborane-Containing Polyfluorene: o-Carborane in the Main Chain. *Macromolecules* 2009;**42**:8594-98.
25. Kokado K, Chujo Y. Multicolor Tuning of Aggregation-Induced Emission through Substituent Variation of Diphenyl-o-carborane. *J Org Chem* 2011;**76**:316-19.

26. Vives G, Tours JM. Synthesis of Single-Molecule Nanocars. *Acc Chem Res* 2009;**43**:473-87.
27. Morin JF, Shirai Y, Tour JM. En Route to a Motorized Nanocar. Org Lett 2006;**8**:1713-16.
28. Kahlert JU, Rawal A, Hook JM, Rendina LM, Choucair M. Carborane functionalization of the aromatic network in chemically-synthesized graphene. *Chem Commun* 2014;**50**:11332-34.
29. Núñez R, Romero I, Teixidor F, Viñas C. Icosahedral boron clusters: a perfect tool for the enhancement of polymer features. *Chem Soc Rev* 2016;**45**:5147-73.
30. Fox MA, Hughes A.K. Cage C-H···X interactions in solid-state structures of icosahedral carboranes. *Coord Chem Rev* 2004;**248**:457-76.
31. Saha A, Oleshkevich E, Viñas C, Teixidor F. Biomimetic Inspired Core-Canopy Quantum Dots: Ions Trapped in Voids Induce Kinetic Fluorescence Switching. *Adv Mater* 2017;**29**:1704238.
32. Hardie MJ, Raston CL. Solid state supramolecular assemblies of charged supermolecules (Na[2.2.2]cryptate)+ and anionic carboranes with host cyclotriveratrylene. *Chem Commun* 2001;**10**:905-06.
33. Yao Z-J, Jin GX. Transition metal complexes based on carboranyl ligands containing N, P, and S donors: Synthesis, reactivity and applications. *Coord Chem Rev* 2013;**257**:2522-35.

34. Scheer M, Schindler A, Groger C, Virovets AV, Peresypkina EV. A Spherical Molecule with a Carbon-Free Ih-C80 Topological Framework. *Angew Chem Int* Ed 2009;**48**:5046-49.

35. Núñez R, Farrás P, Teixidor F, Viñas C, Sillanpää R, Kivekäs R. A Discrete P···I-I···P Assembly: The Large Influence of Weak Interactions on the 31P NMR Spectra of Phosphane–Diiodine Complexes. *Angew Chem Int Ed* 2006;**45**:1270-72.

36. Teixidor F, Barbera G, Vaca A, Kivekäs R, Sillanpää R. Are Methyl Groups Electron-Donating or Electron-Withdrawing in Boron Clusters? Permethylation of o-Carborane. *J Am Chem Soc* 2005;**127**:10158-59.

37. Spokoyny AM, Machan CW, Clingerman DJ, Rosen MS, Wiester MJ, Kennedy RD, et al. A coordination chemistry dichotomy for icosahedral carborane-based ligands. *Nat Chem* 2011;**3**, 590-96.

38. Sun T, Li YY, Huang YL, Zhang ZZ, Yang WL, Du ZW, et al. Targeting glioma stem cells enhances anti-tumor effect of boron neutron capture therapy. *Oncotarget* 2016;**7**:43095-08.

39. Gao ZY, Horiguchi Y, Nakai K, Matsumura A, Suzuki M, Ono K, et al. Use of boron cluster-containing redox nanoparticles with ROS scavenging ability in boron neutron capture therapy to achieve high therapeutic efficiency and low adverse effects. *Biomaterials* 2016;**104**:201-12.

40. Heber EM, Hawthorne MF, Kueffer PJ, Garabalino MA, Thorp SI, Pozzi ECC, et al. Therapeutic efficacy of boron neutron capture therapy mediated by boron-

rich liposomes for oral cancer in the hamster cheek pouch model. *Proc Natl Acad Sci U.S.A* 2014;**111**:16077-81.

41. Xuan S, Zhao N, Zhou ZH, Fronczek FR, Vicente MGH. Synthesis and in Vitro Studies of a Series of Carborane-Containing Boron Dipyrromethenes (BODIPYs). *J Med Chem* 2016;**59**:2109-17.
42. Cioran AM, Musteti AD, Teixidor F, Krpetić Ž, Prior IA, He Q, Kiely CJ, et al. Mercaptocarborane-Capped Gold Nanoparticles: Electron Pools and Ion Traps with Switchable Hydrophilicity. *J Am Chem Soc* 2012;**134**:212-21.
43. Neutron Capture Therapy. Principles and Applications. (Eds: Sauerwein WAG, Wittig A, Moss R, Nakagawa Y), Springer Science & Business Media 2012.
44. Bialek-Pietras M, Olejniczak AB, Tachikawa S, Nakamura H, Lesnikowski ZJ. Towards new boron carriers for boron neutron capture therapy: Metallacarboranes bearing cobalt, iron and chromium and their cholesterol conjugates. *Bioorg Med Chem* 2013;**21**(5):1136-42.
45. Sun T, Li YY, Huang YL, Zhang ZZ, Yang WL, Du ZW, et al. Targeting glioma stem cells enhances anti-tumor effect of boron neutron capture therapy. *Oncotarget* 2016;**7**:43095-08.
46. Calabrese G, Daou A, Rova A, Tseligka E, Vizirianakis IS, Fatouros DG, Tsibouklis J. Boron-containing delocalised lipophilic cations for the selective targeting of cancer cells. *Med Chem Commun* 2017;**8**, 67-72.
47. Nedunchezhian K., Aswath N., Thiruppathy M., Thirugnanamurthy S. Boron Neutron Capture Therapy. J Clin Diagn Res. 2016; 10(12):ZE01–ZE04.

48. Oleshkevich E, Teixidor F, Rosell A, Viñas C. Merging Icosahedral Boron Clusters and Magnetic Nanoparticles: Aiming toward Multifunctional Nanohybrid Materials. *Inorg Chem* 2018;**57**:462-70.
49. Carenza E, Barceló V, Morancho A, Levander L, Boada C, Laromaine A, et al. In vitro angiogenic performance and in vivo brain targeting of magnetized endothelial progenitor cells for neurorepair therapies. *Nanomedicine NBM* 2014;**10**(1):225-34.
50. Matuszak J, Zaloga J, Friedrich RP, Lyer S, Nowak J, Odenbach S, et al. Endothelial biocompatibility and accumulation of SPION under flow conditions. *J Magn Magn Mater* 2015;**380**:20-26.
51. Sundstrøm T, Daphu I, Wendelbo I, Hodneland E, Lundervold A, Immervoll H, et al. Automated Tracking of Nanoparticle-labeled Melanoma Cells Improves the Predictive Power of a Brain Metastasis Model. *Cancer Res* 2013;**73**:2445-56.
52. Lu X, Liu W, Ouyang J, Tian Y. Distinct surface hydration behaviours of boron-rich boride thin film coatings. *Appl Surf Sci* 2014;**311**:749-52.
53. M Wang Y-XJ. Superparamagnetic iron oxide based MRI contrast agents: Current status of clinical application. *Quant Imaging Med Surg* 2011;**1**:35-40.
54. Geninatti-Crich S, Alberti D, Szabo I, Deagostino A, Toppino A., Barge A, et al. MRI-guided neutron capture therapy by use of a dual gadolinium/boron agent targeted at tumour cells through upregulated low-density lipoprotein transporters. *Chemistry* 2011;**17**(30):8479-86.

55. Deagostino A, Protti N, Alberti D, Boggio P, Bortolussi S, Altieri S, et al. Insights into the use of gadolinium and gadolinium/boron-based agents in imaging-guided neutron capture therapy applications. *Future Med Chem* 2016;**8**(8):899-917.

56. Aires A, Ocampo SM, Cabrera D, de la Cueva L, Salas G, Teran FJ, et al. BSA-coated magnetic nanoparticles for improved therapeutic properties. *J Mater Chem* B 2015;**3**:6239-47.

57. Salvati A, Pitek AS, Monopoli MP, Prapainop K, Bombelli FB, Hristov DR, et al. Transferrin-functionalized nanoparticles lose their targeting capabilities when a biomolecule corona adsorbs on the surface. *Nat Nanotechnol* 2013;**8**(2):137-43.

58. Angelopoulos I, Southern P, Pankhurst QA, Day RM. Superparamagnetic iron oxide nanoparticles regulate smooth muscle cell phenotype. *J Biomed Mater Res A* 2016;**104**:2412-19.

59. Wilhelm C, Gazeau F. Universal cell labelling with anionic magnetic nanoparticles. *Biomaterials* 2008;**29**:3161-74.

60. Barth RF, Vicente GMH, Harling OK, Kiger III WS, Riley KJ, Binns PJ,et al. Current status of boron neutron capture therapy of high grade gliomas and recurrent head and neck cancer. *Radiat Oncol* 2012;**7**:146-67.

Figure legends

Figure 1. Schematic representation of *m*-carborane, *m*-carboranylphosphinic acid (H[**1**]), its sodium salt (Na[**1**]), and bidentate bridging coordination mode of [**1**]$^-$ onto the MNPs' surface.

Figure 2. Cell viability was tested after exposing brain endothelial cells (A), and Glioblastoma cells (B) to increasing doses of **1**-MNPs and corresponding vehicle solutions for 24 hours. Data is expressed as mean ±SD of n=3/4 per condition; * $p<0.05$ indicates differences vs. control media (dashed line). Right panels correspond to images of each cell line (a) and to iron deposits observed after Prussian Blue Stain (b, treatment dose 10 μg/mL).

Figure 3. The amount of $Fe^{2+/3+}$ per viable cell was determined after treating cells with increasing doses of **1**-MNPs for 6 or 24 hours. Bar graph (A) shows that the amount of Fe/cell was time- and dose-dependent in both cell lines. The tested glioblastoma cells (A172) were capable to uptake the largest amounts of iron at all sub-toxic tested doses (B). Data is expressed as mean ±SD pg $Fe^{2+/3+}$/Cell of n=3 independent experiments per condition.

Figure 4. Transmission electron microscope (TEM) image of A) glioblastoma cells (A172) and B) endothelial hCMEC/D3 cells showing the presence of **1**-MNPs into the cytoplasm with a larger load in A172cells. Glioblastoma cells (A) were also

imaged by T_2-weighted MRI at 7T in glass capillaries containing cell pellets of untreated A172 cells (1) or A172 cells incubated for 6h with 25 or 50 µg Fe/mL **1**-MNPs (2 and 3, respectively) or for 24h with 25 or 50 µg Fe/mL NPs (4 and 5, respectively).

Figure 5. High resolution spectra XPS of **1**-MNPs and A172 cells treated with 1-MNPs (A) in the B 1s and P 2p regions, (B) and (C), respectively**.**

Figure 6. Cell viability after exposing brain endothelial cells (hCMEC/D3) and glioblastoma cells (A172) to increasing concentrations of the Na[**1**] salt compared to control treatment (vehicle). A) bar graph representing cell viability after 24 h treatment (mean ±SD). B) Representative images of cells after MTT assay**.**

Figure 7. Proliferation curves of A172 cells re-plated one day after BNCT treatment. Data are the mean ± SD of two different experiments.

Figure 8. Mouse weight after *in vivo* administration of **1**-MNPs or vehicle in mice. (A) Mice were weighted before **1**-MNPs (n=6) or Vehicle (n=7) intravenous administration, and followed up at 1, 2, 3 and 10 days of injection. A group of naïve mice who did not receive any treatment were also weighted at the same days (n=3). (B) The Individual weight increase or decrease at day 10 was calculated for each mouse and represented, showing no differences between treatment groups**.**

Table 1. Hydrodynamic diameter and diffusion coefficients values of **1**-MNPs suspensions at different culture media and temperatures (r.t. and 37°C) measured by DLS.

Media	T, ºC	$Ø_{HYD}$, (nm)	Diffusion Coefficient, (m^2/s)
		10 min	
DMEM F12–1% FBS	r.t	9.8 ± 2.5	3.40
	37	8.2 ± 2.6	3.63
EGM-2 medium with 2%FBS;	r.t	90.3 ± 40.7	4.43
	37	98.7 ± 41.6	5.69
DMEM-1% FBS	r.t	103.4 ± 40.7	4.14
	37	106.6 ± 42.9	5.13
RPMI	r.t	9.0 ± 2.3	4.16
	37	8.4 ± 2.0	4.19
PBS	r.t	76.1 ± 31.1	4.90
		24 hours	
DMEM F12–1% FBS	r.t	9.5 ± 2.2	3.50
	37	8.5 ± 2.3	4.03
EGM-2 medium with 2%FBS;	r.t	99.5 ± 41.9	4.31
	37	101.0 ± 42.6	5.54
DMEM-1% FBS	r.t	123.6 ± 40.8	3.42
	37	133.3 ± 43.4	4.24

RPMI	r.t	10.8 ± 4.4	3.92
	37	11.0 ± 12.9	4.09
PBS	1276 ± 435 (precipitated)		

Figure 1.

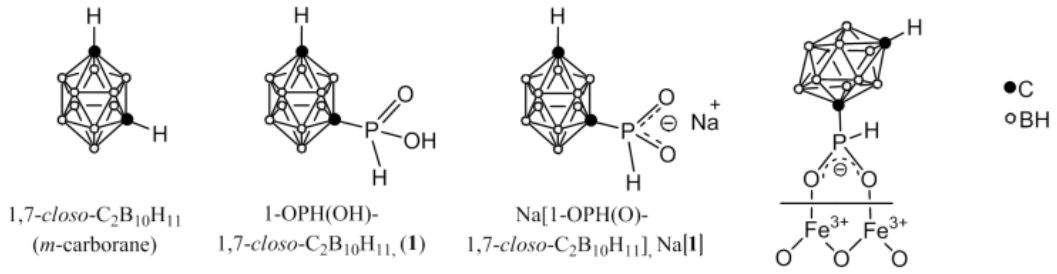

1,7-*closo*-$C_2B_{10}H_{11}$ (*m*-carborane)

1-OPH(OH)-1,7-*closo*-$C_2B_{10}H_{11}$, (**1**)

Na[1-OPH(O)-1,7-*closo*-$C_2B_{10}H_{11}$], Na[**1**]

Figure 2.

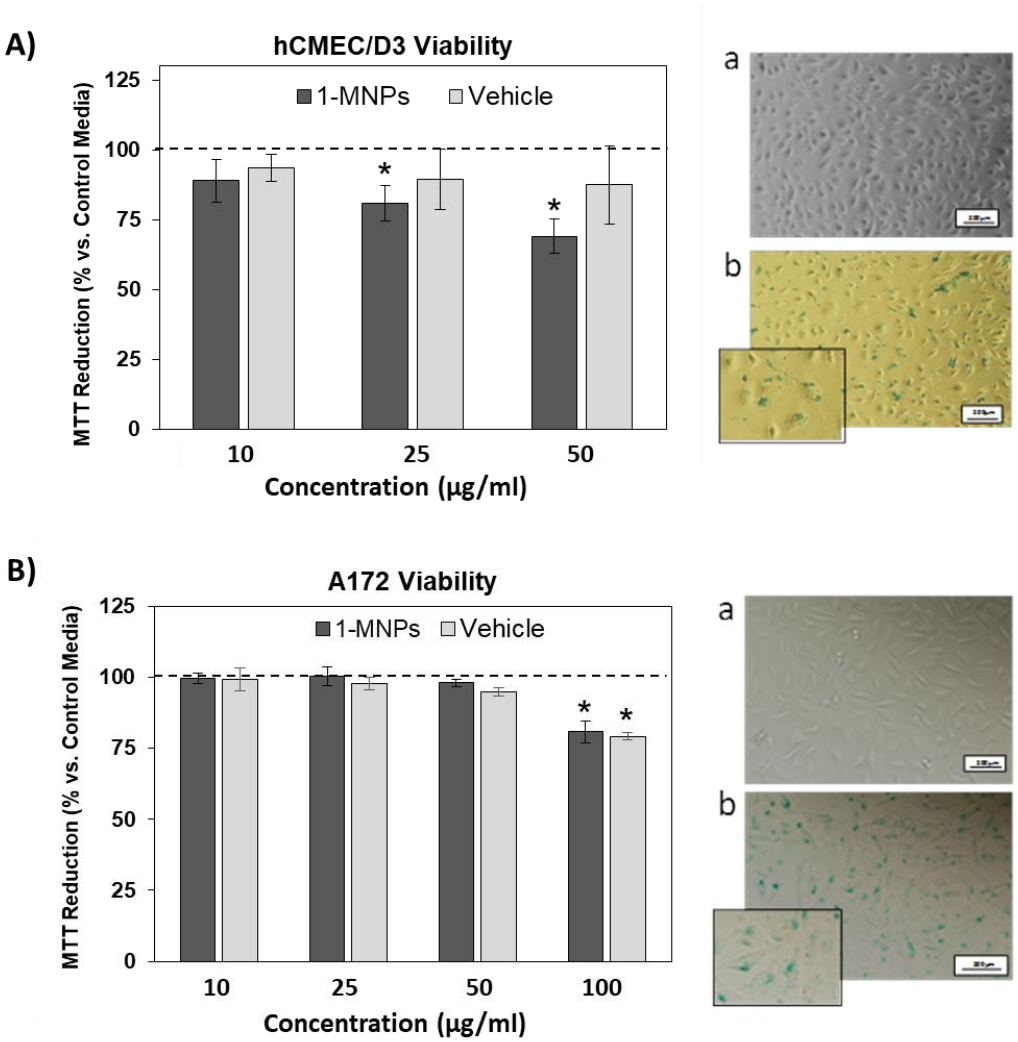
A)
hCMEC/D3 Viability
1-MNPs
Vehicle
MTT Reduction (% vs. Control Media)
125
100
75
50
25
0
10
25
50
Concentration (µg/ml)
a
b
B)
A172 Viability
1-MNPs
Vehicle
MTT Reduction (% vs. Control Media)
125
100
75
50
25
0
10
25
50
100
Concentration (µg/ml)
a
b

Figure 3.

A

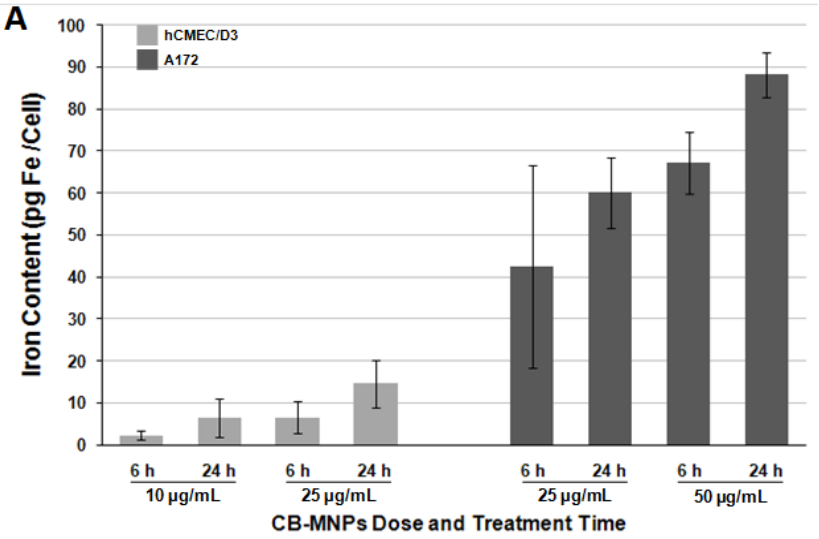

B

	hCMEC/D3				A172			
	10µg/mL		25µg/mL		25µg/mL		50µg/mL	
	6h	24h	6h	24h	6h	24h	6h	24h
MEAN	2.32	6.56	6.61	14.66	42.49	60.07	67.38	88.26
SD	1.16	4.52	3.73	5.69	24.14	8.27	7.33	5.37

Figure 4.

A)

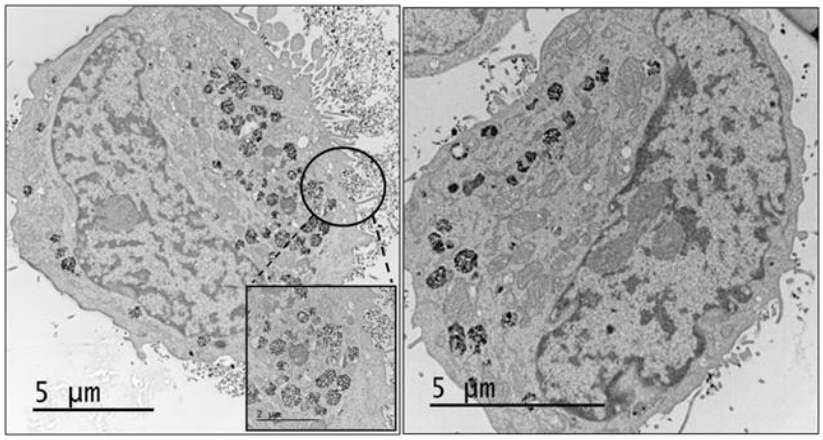

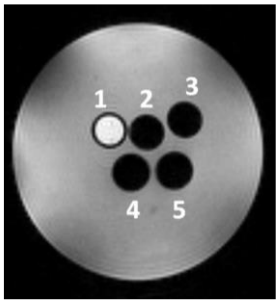

B)

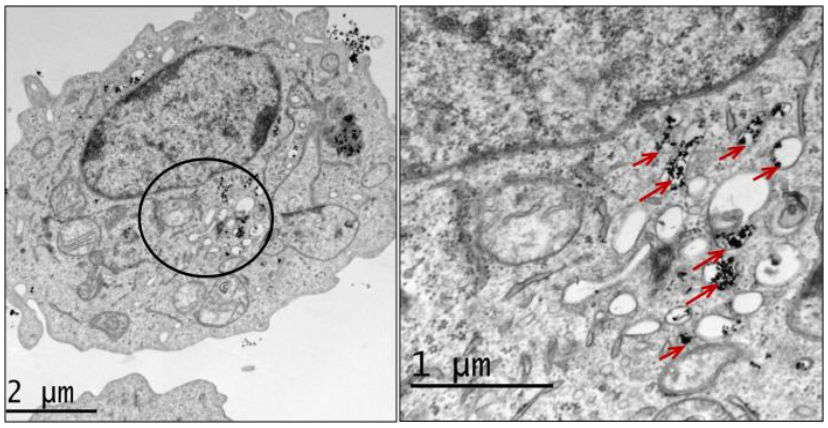

Figure 5.

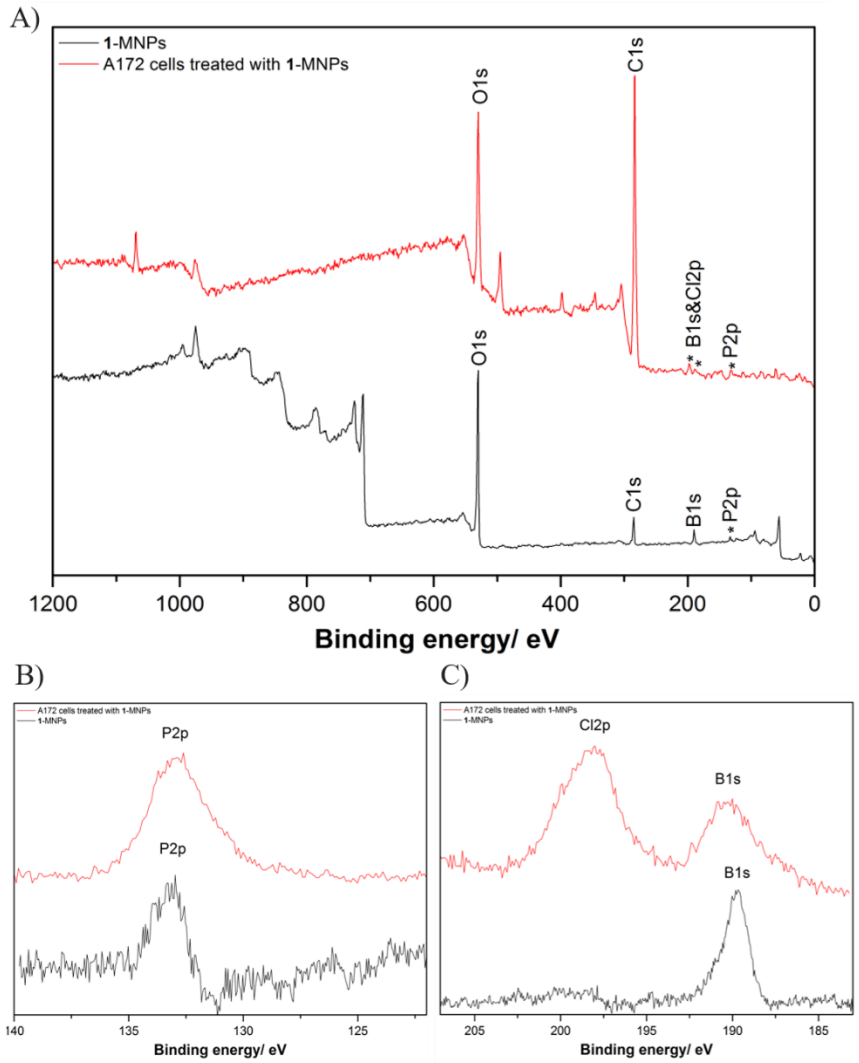
A)
1-MNPs
A172 cells treated with 1-MNPs
O1s
C1s
B1s&Cl2p
P2p
O1s
C1s
B1s
P2p
1200
1000
800
600
400
200
0
Binding energy/ eV
B)
A172 cells treated with 1-MNPs
1-MNPs
P2p
P2p
140
135
130
125
Binding energy/ eV
C)
A172 cells treated with 1-MNPs
1-MNPs
Cl2p
B1s
B1s
205
200
195
190
185
Binding energy/ eV

Figure 6.

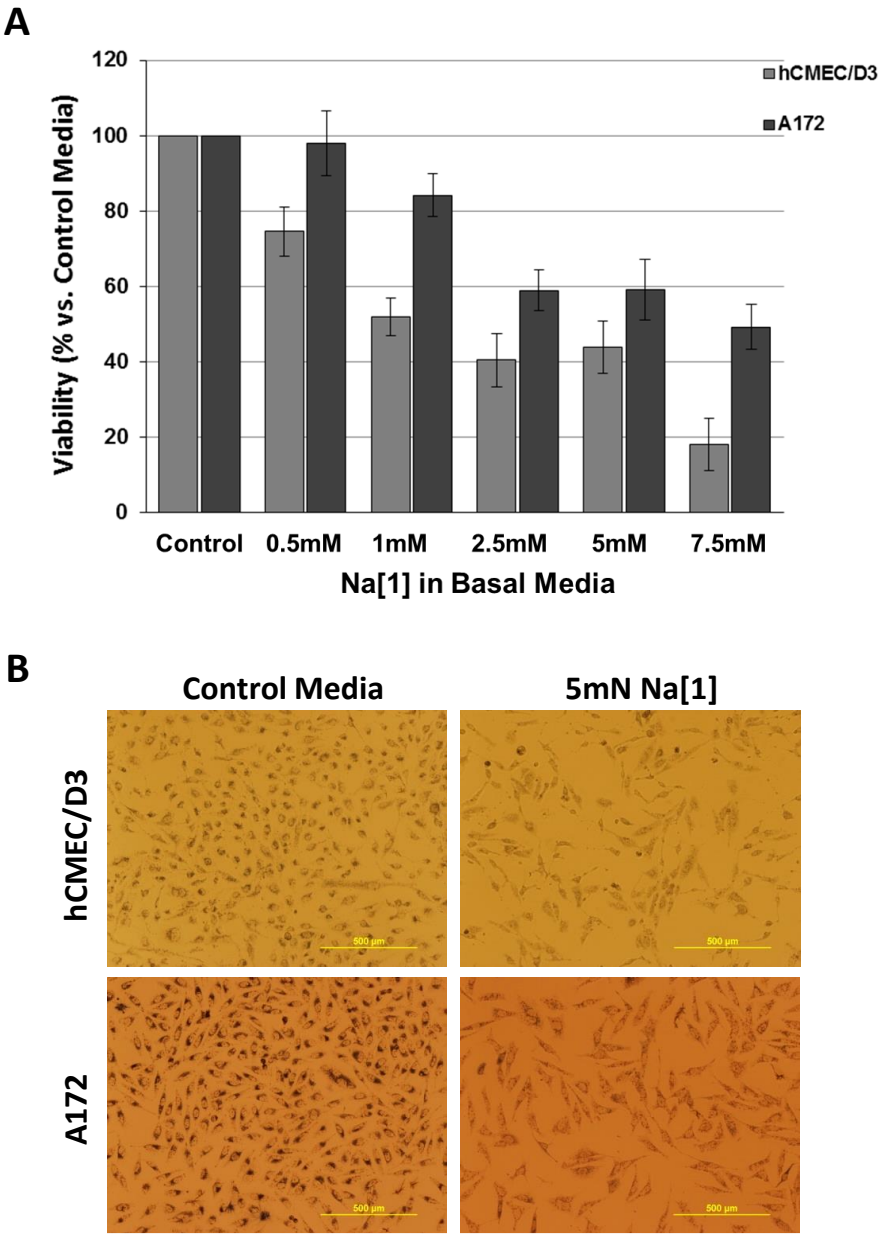
A
120
100
80
60
40
20
0
Viability (% vs. Control Media)
hCMEC/D3
A172
Control
0.5mM
1mM
2.5mM
5mM
7.5mM
Na[1] in Basal Media
B
Control Media
5mN Na[1]
hCMEC/D3
A172
500 µm

Figure 7.

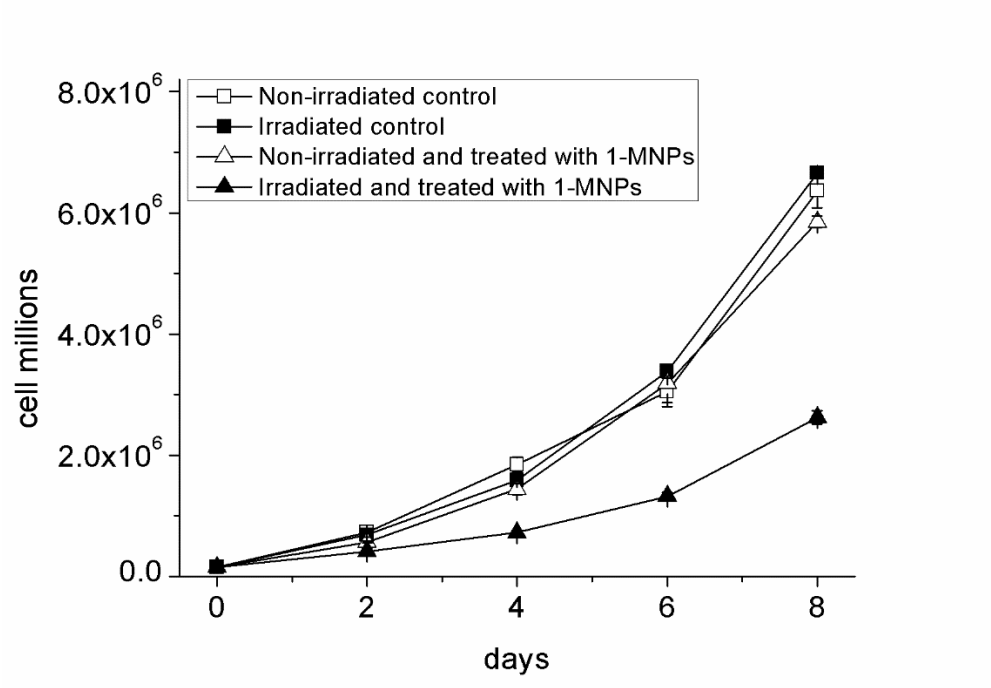
Non-irradiated control
Irradiated control
Non-irradiated and treated with 1-MNPs
Irradiated and treated with 1-MNPs
cell millions
8.0x10^6
6.0x10^6
4.0x10^6
2.0x10^6
0.0
0
2
4
6
8
days

Figure 8.

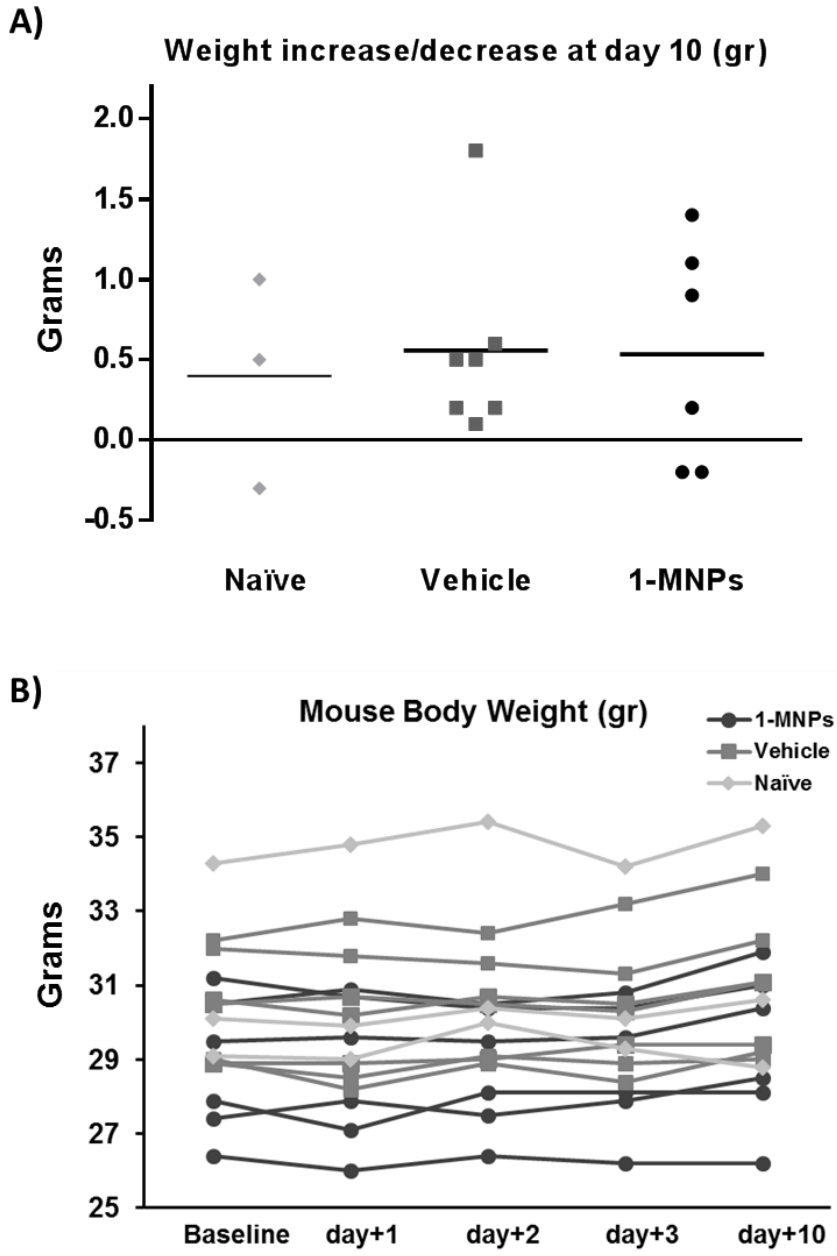
A)
Weight increase/decrease at day 10 (gr)
Grams
2.0
1.5
1.0
0.5
0.0
-0.5
Naïve
Vehicle
1-MNPs
B)
Mouse Body Weight (gr)
1-MNPs
Vehicle
Naïve
Grams
37
35
33
31
29
27
25
Baseline
day+1
day+2
day+3
day+10